Stochastic multiresonance in a chaotic map with fractal basins of attraction

S. Matyjaśkiewicz,[1,2] A. Krawiecki,[1] J. A. Hołyst,[1,2,3] K. Kacperski,[3,1] and W. Ebeling[2]
[1]*Faculty of Physics, Warsaw University of Technology Koszykowa 75, PL-00-662 Warsaw, Poland*
[2]*Institute of Physics, Humboldt University at Berlin, Invalidenstraße 110, D-10115 Berlin, Germany*
[3]*Max Planck Institute for the Physics of Complex Systems, Nöthnitzerstraße 38, D-01187 Dresden, Germany*
(Received 11 August 2000; published 25 January 2001)

Noise-free stochastic resonance in a chaotic kicked spin model at the edge of the attractor merging crisis is considered. The output signal reflects the occurrence of crisis-induced jumps between the two parts of the attractor. As the control parameter—the amplitude of the magnetic field pulses—is varied, the signal-to-noise ratio shows plateaus and multiple maxima, thus stochastic multiresonance is observed. It is shown that the multiresonance occurs due to a fractal structure of the precritical attractors and their basins. In the adiabatic approximation theoretical expression for the signal-to-noise ratio is derived, based on the theory of oscillations in average crisis-induced transient lifetimes. Numerical and theoretical results agree quantitatively just above the threshold for crisis and qualitatively in a wide range of the control parameter.

DOI: 10.1103/PhysRevE.63.026215 PACS number(s): 05.45.−a, 05.40.−a

I. INTRODUCTION

Stochastic resonance (SR) [1] is a phenomenon occurring in certain systems driven by a combination of noise and periodic signal, whose essence is that the input noise intensity can be tuned to maximize the degree of periodicity of a properly defined output signal (for recent reviews see [2,3]). A similar phenomenon, called noise-free SR, occurs in chaotic periodically driven systems in which, in the absence of external noise, the internal chaotic dynamics can be changed by varying the control parameter so that the periodic signal is best transmitted [4–15]. In systems with SR the power spectrum density (PSD) of the output signal consists of peaks at the multiples of periodic forcing frequency superimposed on a broadband noise background. The best transmission of the periodic signal is thus defined as the maximization of the output signal-to-noise ratio (SNR), i.e., the ratio of the height of the peak at the periodic forcing frequency to the height of the noise background. Usually only one maximum of the SNR is observed as the input noise intensity or the control parameter in a chaotic system is varied. However, in Ref. [16] a second small maximum for small noise intensity was observed. Recently it has been also found that in certain systems many or even an infinite number of maxima of the output SNR can appear. This phenomenon is called stochastic multiresonance [17,18].

Although the first studies of SR and noise-free SR were performed in dynamical systems with bistable potential [4,5,11,12,16,19–21] SR is now equally well investigated in dynamical and nondynamical threshold-crossing (TC) systems [9,10,13,22–28]. As TC systems we understand systems with output in the form of pulses emitted each time when a certain threshold is crossed. E.g., the membrane potential of a neuron under the influence of external noise and periodic stimulus can increase rapidly above the threshold voltage so that a single pulse of neural activity is emitted, after which the membrane potential is reset to the resting value [22,28]. Dynamical systems with symmetric bistable potential can be also described as TC systems if the noise and periodic signal change the height of the potential barrier, or the depth of the two potential wells in a symmetric manner. The TC events are then jumps of the particle over the barrier between potential wells, and the output signal is defined in such a way that every jump triggers a single pulse in the otherwise zero signal. This is in contrast with the abovementioned first models of SR in bistable systems in which the relative depth of the two potential wells is changed by noise and periodic modulation, and the output signal reflects the position of the particle in the left or right well [20]. SR in TC systems is observed if the SNR evaluated from the output pulse train shows a maximum as a function of the input noise intensity.

The aim of the present paper is to investigate noise-free stochastic multiresonance in a TC system. For this purpose we study a chaotic map that models the dynamics of a damped classical magnetic moment (spin) driven by pulses of magnetic field in the presence of anisotropy [29–34]. At a certain value of the amplitude of such pulses the attractor merging crisis [35] occurs and jumps of the spin vector between two parts of the postcritical chaotic attractor corresponding to two equivalent spin orientations become possible [29,30]. When the amplitude of pulses is modulated by additional periodic signal the map can be described as a bistable dynamical TC system in which the jumps between the two parts of the attractor are TC events. SR induced by external noise was studied by us in such a model in Ref. [34]. Here we are interested in the case without noise. In contrast, the role of noise is played by deterministic chaos, and instead of varying the noise intensity we change the system control parameter, i.e., the mean value of the amplitude of pulses. Our numerical simulations show that the SNR depends on the control parameter in a very complicated way, i.e., one observes multiple strong maxima (noise-free stochastic multiresonance) and various small plateaus and local maxima. We show that this phenomenon is a direct consequence of the fractal structure of the precritical attractors and their basins of attraction leading to oscillations in the average time between jumps between the two parts of the postcritical attractor [32,33]. Our theoretical results, based on the model

of such fractal structures, describe qualitatively the results of numerical simulations.

II. MODEL

We consider a classical magnetic moment (spin) $\mathbf{S}$, $|\mathbf{S}|=S$ in the uniaxial anisotropy field and external transverse magnetic field $\tilde{B}(t)$ parallel to the x axis [29–34]. The system is described by the Hamiltonian

$$H=-A(S_z)^2-\tilde{B}(t)S_x \tag{1}$$

where $A>0$ is the anisotropy constant. The motion of the spin is determined by the Landau-Lifschitz equation with damping term

$$\frac{d\mathbf{S}}{dt}=\mathbf{S}\times\mathbf{B}_{eff}-\frac{\lambda}{S}\mathbf{S}\times(\mathbf{S}\times\mathbf{B}_{eff}), \tag{2}$$

where $\mathbf{B}_{eff}=-dH/d\mathbf{S}$ is the effective magnetic field and $\lambda>0$ is the damping parameter. Taking the transverse field in the form of periodic δ pulses with amplitude B and period $\tilde{\tau}$,

$$\tilde{B}(t)=B\sum_{n=1}^{\infty}\delta(t-n\tilde{\tau}), \tag{3}$$

and using the fact that S is constant, Eq. (2) can be integrated in two steps. In the time between pulses of the magnetic field the spin performs damped precession and approaches the anisotropy axis. During the action of the magnetic field the anisotropy can be neglected and the spin performs precession around the x axis tilting towards it at the same time. The result of the integration can be written as a superposition of two two-dimensional maps T_A and T_B. The map T_A describes the time evolution between kicks,

$$T_A\begin{bmatrix}\phi\\ S_z\end{bmatrix}=\begin{bmatrix}\phi+\Delta\phi\\ WS_z\end{bmatrix}, \tag{4}$$

where ϕ is the angle between the x axis and the projection of the spin on the x-y plane and

$$\Delta\phi=(1/\lambda)\ln\{(1+S/S_z)/[1+S/(WS_z)]\}-2AS\tilde{\tau},$$

$W=[c^2+(S_z/S)^2(1-c^2)]^{-1/2}$, $c=\exp(-2\lambda AS\tilde{\tau})$. The map T_B written in the variables (S_x,Φ), where Φ is the angle between the y axis and the projection of the spin on the x-z plane, describes the motion of the spin during the action of the field pulses and has a form

$$T_B\begin{bmatrix}\Phi\\ S_x\end{bmatrix}=\begin{bmatrix}\Phi-B\\ S-2S(S-S_x)D^2U\end{bmatrix}, \tag{5}$$

where $D=\exp(-\lambda B)$ and $U=[S+S_x+D^2(S-S_x)]^{-1}$. The complete dynamics is a superposition of both maps

$$\mathbf{S}_{n+1}=T_B[T_A[\mathbf{S}_n]], \tag{6}$$

where $\mathbf{S}_n$ is a spin vector just after the action of the nth magnetic field pulse.

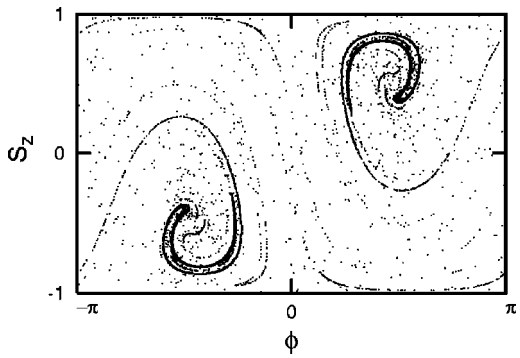

FIG. 1. Attractor of the spin map (6) with $S=1$, $A=1$, $\tilde{\tau}=2\pi$, $\lambda=0.105\,494\,2$, $B_c=1$, and $B=1.0001>B_c$.

The classical model described by Eqs. (1)–(6) is related to experimentally investigated quantum magnetic systems, if one considers the properties of isolated spins of large magnetic molecules such as $Mn_{12}O_{12}(CH_3COO)_{16}$ where the anisotropy is induced by molecule symmetry [36] or the nanometric-size single domain ferromagnetic particles (superparamagnets) used for the observation of the macroscopic quantum tunneling phenomenon [37]. The quantum version of this model (sometimes called the kicked top model) is an interesting system from the point of view of quantum chaos; corresponding quasienergy statistics, level dynamics, and decoherence effects have been studied in detail in Refs. [38–40]. It should also be mentioned that SR in a ferrite-garnet film with uniaxial anisotropy, connected with magnetization tunneling due to thermal fluctuations or external noise was studied experimentally in Refs. [41,42], but in the presence of sinusoidal magnetic field rather than field kicks with modulated amplitude.

The map (6) exhibits a rich variety of periodic and chaotic dynamics. Let us take B as the control parameter and consider the map (6) with parameters $S=1$, $\tilde{\tau}=2\pi$, $\lambda=0.105\,494\,2$ and $A=1$. For B slightly below $B_c=1$ two symmetric chaotic attractors of Eq. (6) corresponding to two spin orientations (spin ''up,'' $S_z>0$ and ''down,'' $S_z<0$) in the absence of the external field exist [29,30]. For $B>B_c$ these two attractors merge as a result of the attractor merging crisis [31–33] and a new postcritical attractor (Fig. 1) consisting of two symmetric parts is born. The system switches chaotically between these two parts and the mean time between switches $\langle\tau\rangle$ as a function of the control parameter B obeys a power scaling law [35,43] $\langle\tau(B)\rangle\propto(B-B_c)^{-\eta}$, where $\eta>0$ is a critical exponent. However, there are also considerable oscillations superimposed on this trend [32,33]. They are connected with the fractal structure of precritical attractors and their basins of attraction. In general, for various parameter values, two kinds of such oscillations can be distinguished. If the basins of attraction do not have a self-similar (fractal) structure the so-called normal oscillations are observed, induced by consecutive branches of the fractal attractor creeping, with increasing control parameter, into the nonfractal basin of attraction of another attractor [33], which results in the modulation of the slope of $\langle\tau(B)\rangle$. When the basins of attraction are fractal sets anomalous oscillations appear, including sections where $\langle\tau(B)\rangle$ increases against

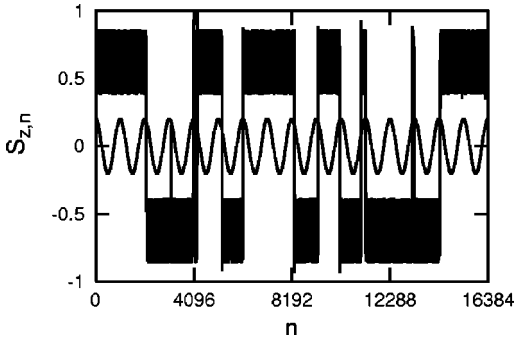

FIG. 2. Time series S_z vs n of the spin map (6) with parameters as in Fig. 1 and $B_1=6\times10^{-4}$, $T_0=1024$, $B_0=0.9999$. Also a periodic signal proportional to $B_1\cos\omega_0 n$ is shown. It can be seen that the jumps between the states $S_{z,n}<0$ and $S_{z,n}>0$ occur most probably when the periodic signal is at a maximum.

the general trend [32]. Typically their magnitude is larger than that of normal oscillations.

In order to observe noise-free SR we investigate the system (2) driven by the magnetic field pulses (3) whose amplitude B is no longer constant but periodically modulated in time with frequency $\tilde{\omega}_0$ [we denote this time-dependent amplitude as $B(t)$]. The period of this modulation $2\pi/\tilde{\omega}_0$ is assumed as an integer multiple of $\tilde{\tau}$. The resulting dynamics can be again rewritten in the form of a map (6), but with periodically modulated control parameter

$$B(n)=B_0+B_1\cos\omega_0 n, \tag{7}$$

where $\omega_0=\tilde{\omega}_0\tilde{\tau}$ is a dimensionless frequency. In the continuous-time dynamics, Eqs. (1)–(3), due to the periodic character of the magnetic field pulses (3) with period $\tilde{\tau}$, peaks in the power spectrum of the system at the multiples of the frequency $2\pi/\tilde{\tau}$ should appear. Besides, peaks should also appear at the multiples of the modulation frequency of the amplitude of the field kicks $\tilde{\omega}_0$. In the discrete-time system (6) the highest observable frequency corresponds to half of the frequency of the field kicks, so only the latter peaks, at the multiples of ω_0, will be observed. Thus in the discrete-time system SR can be observed at the frequency ω_0 and is connected with the external modulation (7).

Employing the analogy to dynamical systems with bistable potential, the two symmetric parts of the postcritical attractor in our model correspond to two potential wells, and the parameter $B(n)-B_c$ controls the height of the potential barrier. Thus, our system can be described as a dynamical TC system and the spin jumps between the two parts of the postcritical attractor can be treated as TC events [34]. An example of the time series from the map (6) with the control parameter (7) is shown in Fig. 2. To observe the noise-free SR the SNR at the frequency ω_0 is studied as a function of the control parameter B_0. Due to the complex, nonmonotonic dependence of $\langle\tau\rangle$ on B a corresponding complex dependence of the SNR on B_0 is expected.

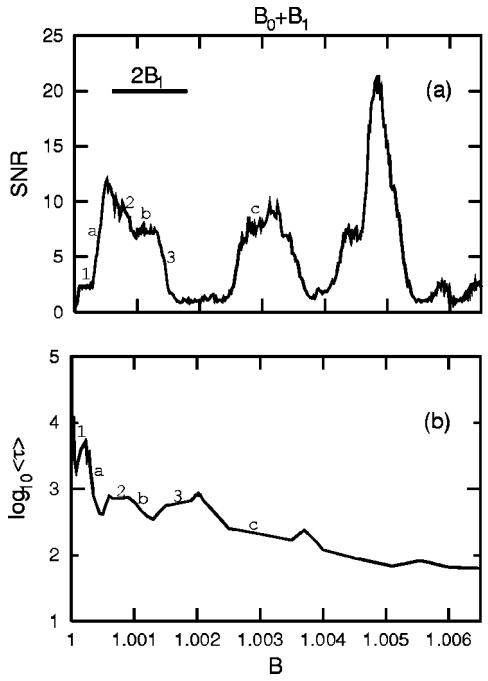

FIG. 3. (a) The SNR vs B_0+B_1 for the signal y_n from the spin map (6) with parameters as in Fig. 1 and $B_1=6\times10^{-4}$, $T_0=1024$. (b) The mean time between jumps between symmetric parts of the attractor $\langle\tau\rangle$ vs B for the spin map (6) with parameters as in Fig. 1; anomalous oscillations can be seen. The labeled segments in (a) and (b) correspond to each other according to the heuristic rules discussed in Appendix A [segment 2 in (b) is a composite segment consisting of a rising and flat part].

III. NUMERICAL SIMULATIONS: AN EXAMPLE OF NOISE-FREE STOCHASTIC MULTIRESONANCE

In this section numerical results concerning SR in the system (6) are presented. We define the output signal so that pulses of unit height correspond to the jumps between the two parts of the postcritical attractor: $y_n=1$ if at iteration n the jump occurred and $y_n=0$ otherwise. Due to the symmetry of the system with respect to the plane $S_z=0$ we can assume that the jump occurs when $S_{z,n-1}$ and $S_{z,n}$ have opposite signs. As a measure of noise-free SR we take the output SNR as a function of B_0. The output PSD $S(\omega)$ is calculated from 2^{15} points of the signal y_n and the SNR is evaluated as

$$\mathrm{SNR}=S_P(\omega_0)/S_N(\omega_0), \tag{8}$$

where $S_N(\omega_0)$ is the noise background in the vicinity of ω_0 and $S_P(\omega_0)=S(\omega_0)-S_N(\omega_0)$ is the height of the peak in the PSD at $\omega=\omega_0$. It should be remembered that due to finite frequency resolution Δf (here, $\Delta f=2^{-15}$) the value of the SNR evaluated from numerical simulations as in Eq. (8) is increased by the factor $1/\Delta f=2^{15}$ in comparison with its true value [20]. This is taken into account when comparing the numerical and theoretical results in Secs. IV–VI.

In Fig. 3(a) a typical curve SNR vs B_0 is shown for a slowly varying input signal with period $T_0=2\pi/\omega_0=1024$ and amplitude $B_1=6\times10^{-4}$. Jumps between symmetric

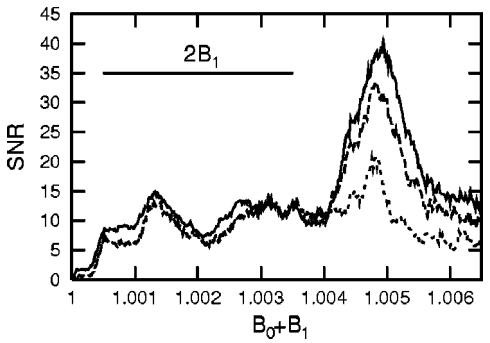

FIG. 4. The SNR vs B_0+B_1 for the signal y_n from the spin map (6) with parameters as in Fig. 1 and with $B_1=1.5\times10^{-3}$, for $T_0=8$ (dotted curve), $T_0=16$ (dashed curve), and $T_0=32$ (solid curve).

parts of the postcritical attractor, and thus a nonzero SNR, are observed for $B_0>B_c-B_1=0.9994$. Within the range of B_0 shown in Fig. 3(a) the curve exhibits three strong maxima, so the noise-free stochastic multiresonance is found. These maxima are accompanied by numerous tiny local maxima and plateaus (flat narrow segments on the slopes of strong maxima).

In Fig. 3(b) the corresponding curve $\langle\tau\rangle$ vs B is shown (without modulation). A closer inspection of Figs. 3(a) and 3(b) reveals that certain segments (the labeled ones) in the two curves can be related to each other. The plateaus and falling segments in Fig. 3(a) turn out to be connected with the rising segments of oscillations in Fig. 3(b) (labeled by numbers), and the rising segments and maxima in Fig. 3(a)—with falling segments of oscillations in Fig. 3(b) (labeled by letters). In Appendix A simple heuristic rules are given, valid for B_0+B_1 close to B_c, which relate the corresponding segments in Figs. 3(a) and 3(b). These rules enable us to predict the location of certain segments in the curves SNR vs B_0 solely on the basis of the measurements of $\langle\tau\rangle$ vs B.

The relationship between the curves SNR vs B_0 and $\langle\tau\rangle$ vs B indicates that the occurrence of noise-free stochastic multiresonance and complicated dependence of the SNR on the control parameter in our model is a result of the fractal structure of precritical attractors and their basins of attraction; this conclusion is further confirmed by the theoretical results of Sec. IV. The infinite self-similar structure of these fractals suggests that the curve SNR vs B_0 is a fractal curve as well and its fine structure can be revealed by measurements of the SNR with higher and higher accuracy. This distinguishes noise-free stochastic multiresonance in our system from stochastic multiresonance induced by external noise, since in the latter case the curves SNR vs noise intensity are smooth [17,18].

In Fig. 4 the curves SNR vs B_0 are shown for $B_1=1.5\times10^{-3}$ and different driving frequencies ω_0. This proves that noise-free stochastic multiresonance occurs also for fast varying periodic signals with relatively large amplitude. As usually, the decrease of the SNR is observed with increasing ω_0, in particular for larger values of B_0.

IV. THEORY FOR THE SIGNAL-TO-NOISE RATIO

A. General formulation

In this section we derive an approximate analytic formula for the SNR vs B_0. It is based on an expression for the SNR in nondynamical discrete-time TC systems [25,26], which, however, can be also applied to dynamical TC systems under the assumption that individual TC events are independent. In our system this assumption means that the average time between jumps is long enough so that the correlations between them are lost, which is true for B_0+B_1 close to B_c. The expression for the SNR is obtained using the periodic in time probability of the TC event $p(n)$. In our case, this probability can be easily evaluated in the adiabatic limit $\omega_0\to0$ and $B_1\ll1$ in which $p(n)=\Pr(y_n=1)=1/\langle\tau(B_0+B_1\cos\omega_0 n)\rangle\equiv1/\langle\tau(n)\rangle$; i.e., it is given by the inverse of the mean time between jumps for the actual value of the control parameter $B(n)$ (7). Hence the following theory is applicable only in the limit of small values of $B_0+B_1-B_c$, B_1 and ω_0.

According to Refs. [25,26] the SNR may be evaluated as

$$\mathrm{SNR}=MT_0|P_1|^2/(\overline{p}-\overline{p^2})\approx MT_0|P_1|^2/\overline{p}, \tag{9}$$

where $P_1=T_0^{-1}\Sigma_{n=0}^{T_0-1}p(n)\exp(-i\omega_0 n)$ is the first Fourier coefficient of $p(n)$, M is the number of periods within the time interval from which the data were stored (in our case, $MT_0=2^{15}$), and the bar denotes the time average over T_0. The approximate equality holds for $p(n)\ll1$, which is the case in our system close to crisis [cf. Fig. 3(b)]. In Eq. (9) the SNR is evaluated taking into account the finite frequency resolution $\Delta f=1/MT_0$ [20] so it can be directly compared to the SNR obtained numerically. Hence in order to evaluate the SNR in the system (6) we need to know $\overline{p}$ and P_1, which can be obtained analytically from a simple model of the attractor merging crisis.

B. Evaluation of the signal-to-noise ratio in a model of fractal attractor and fractal basin of attraction.

In the spin map (6) as the control parameter B is increased above B_c the two precritical attractors $S_z<0$ and $S_z>0$ merge and become chaotic saddles, while their former basins of attraction become pseudobasins (for a more detailed discussion of these concepts see Refs. [32,33]). Due to the system symmetry the pseudobasins are also symmetric, so it is enough to consider only a single chaotic saddle creeping, with the increase of B, into the pseudobasin of the opposite saddle. Henceforth we assume that above the crisis point the structure and measure of chaotic saddles and pseudobasins is identical with that of precritical attractors and their basins at the crisis point, respectively. The only effect of the increase and modulation of the control parameter is the relative shift and modulation of the position of the chaotic saddle with respect to the pseudobasin.

In Refs. [32,33] self-similar models of the chaotic saddle and the pseudobasin have been introduced in order to describe the nonsmooth and nonmonotonic dependence of $\langle\tau\rangle$ on B. Here we implement the model to the case of a periodically modulated control parameter denoted as $q(n)=q_0$

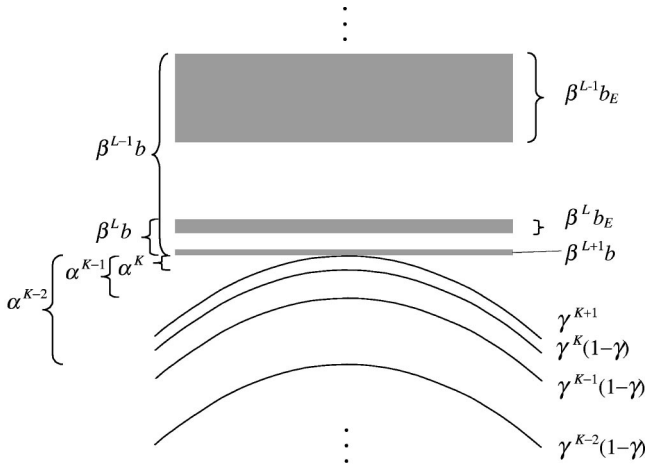

FIG. 5. The model of a fractal chaotic saddle (10) entering the pseudobasin of attraction of the other saddle (11).

$+q_1\cos\omega_0 n$. Following Refs. [32,33] we assume the chaotic saddle $\mathcal{A}$ as a family of $K+2$ parabolic segments $\mathcal{A}_k$ (Fig. 5) moving periodically due to a time-dependent control parameter

$$\mathcal{A}=\bigcup_{k=0}^{K+1}\mathcal{A}_k=\bigcup_{k=0}^{K+1}\{(x,y):y = -x^2-(1-\delta_{k,K+1})a\alpha^k+q_0+q_1\cos\omega_0 n\}, \quad (10)$$

where a and α are model parameters. The invariant measure is uniformly distributed along the parabolic segments and its relative density on the segment A_k is assumed as $\tilde{\mu}_k=(1-\gamma)\gamma^k$ for $0\leqslant k\leqslant K$ and $\tilde{\mu}_{K+1}=\gamma^{K+1}$, where $0<\gamma<1$ is another model parameter. The complicated structure of the pseudobasin is in turn approximated as a family of $L+2$ stripes $\mathcal{B}_l$ accumulating at the line $y=0$ that touches the top of the uppermost parabola A_{K+1} for $q_0=q_1=0$ (Fig. 5)

$$\mathcal{B}=\bigcup_{l=0}^{L+1}\mathcal{B}_l=\bigcup_{l=0}^{L+1}\{(x,y):(1-\delta_{l,L+1})(\beta^l b-\beta^l b_E)\leqslant y\leqslant\beta^l b\}, \quad (11)$$

where β, b, and b_E are again model parameters.

With increasing q_0 the parabolic segments are shifted up and enter the pseudobasin oscillating simultaneously under the influence of the periodic modulation. If we take K and L large enough we get a good approximation of the real system, although in principle one should take K, $L\to\infty$. All model parameters are determined by the fractal structure of the saddles and pseudobasins of the system under study and can be assessed from magnified plots of the collision region between the chaotic saddles and pseudobasins (for details see [32,33]). Besides, the ratio a/b can be treated as a true fitting parameter and chosen so as to obtain the best agreement between the theoretical and numerical values of $\langle\tau\rangle$.

The time-dependent probability of a jump between the symmetric parts of the attractor $p(n)$ is proportional to the time-dependent measure $\mu(n)$ of the overlap of the saddle with the pseudobasin of the other saddle [35,43],

$$p(n)=\zeta\mu(n), \quad (12)$$

where ζ is a proportionality constant. To find $p(n)$ let us first consider the overlap of the kth parabolic segment $\mathcal{A}_k$ with a half-plane $y>c$. The measure of this overlap in the time step n, i.e., the length of the parabola inside the half-plane multiplied by the relative invariant measure density $\tilde{\mu}_k$ will be denoted as $\mu_k[c,n]$. On the basis of Eq. (12) $p(n)$ can be written as a sum of contributions from the individual parabolic segments of the chaotic saddle creeping into the stripes of the pseudobasin

$$p(n)=\zeta\sum_{k=0}^{K+1}\sum_{l=0}^{L+1}\mu_{kl}(n), \quad (13)$$

where

$$\mu_{kl}(n)=\mu_k[(1-\delta_{l,L+1})(\beta^l b-\beta^l b_E),n]-\mu_k[\beta^l b,n]. \quad (14)$$

The time average $\overline{p}$ and the first Fourier coefficient P_1 of the jump probability can also be expressed as double sums

$$\overline{p}=\zeta\sum_{k=0}^{K+1}\sum_{l=0}^{L+1}\overline{\mu}_{kl}, \quad P_1=\zeta\sum_{k=0}^{K+1}\sum_{l=0}^{L+1}M_{kl,1}, \quad (15)$$

where $\overline{\mu}_{kl}$ and $M_{kl,1}$ are the time averages and the first Fourier coefficients of the functions $\mu_{kl}(n)$ [Eq. (14)], respectively. Using the analytic expressions for the time average and the first Fourier coefficient of the function $\mu_k[c,n]$, given in Appendix B, the coefficients $\overline{\mu}_{kl}$ and $M_{kl,1}$ can be also evaluated analytically in the limit of small q_0+q_1. Inserting Eq. (15) into Eq. (9) it is possible to evaluate the SNR vs B_0 numerically for B_0 arbitrarily close to B_c with the accuracy depending on the number of parabolic segments and stripes included in the model. As usually, in the case of adiabatic approximation in TC systems the resulting SNR does not depend on the periodic forcing frequency [23,25] (cf. Appendix B).

C. The origin of multiple maxima

Before comparing the theoretical and numerical results in the next section we discuss qualitatively the origin of multiple maxima appearing in the plots of the SNR vs B_0 like those in Fig. 3(a). Using the just-defined model, let us consider one parabolic segment $\mathcal{A}_0=\{(x,y):y=-x^2+q_0+q_1\cos\omega_0 n\}$, $q_1>0$, with the density $\tilde{\mu}_0=1$ creeping into a single stripe of the pseudobasin $\mathcal{B}_0=\{(x,y):0\leqslant y\leqslant b\}$ as q_0 increases. This means we put $K+1=L+1=0$. The top of the parabola can overlap with the stripe (and thus the SNR is nonzero) if $q_0>-q_1$. The plots of the SNR vs q_0+q_1 obtained from Eq. (9) using Eq. (12) for different b are shown in Fig. 6(a), and the corresponding plots $MT_0|P_1|^2$ vs q_0+q_1 in Fig. 6(b) and $\langle\tau\rangle$ vs q in Fig. 6(c).

If the width of the stripe is very large, $b\gg 2q_1$, the mean time $\langle\tau\rangle$ decreases monotonically with q, while $|P_1|^2$ shows a smooth maximum. As a result, the SNR exhibits a smooth maximum at q_0 slightly above zero (point A in Fig. 6). This

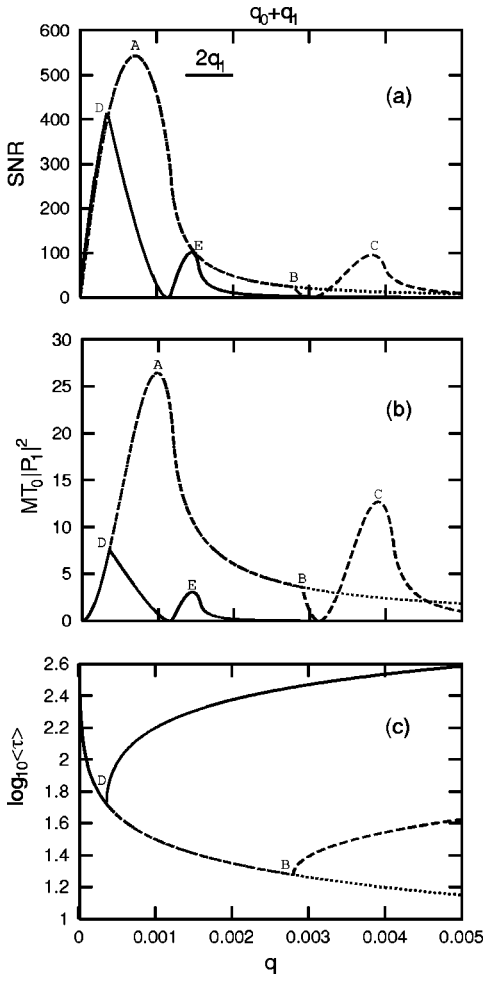

FIG. 6. (a) The SNR vs q_0+q_1 evaluated from Eq. (9) using Eq. (13) with $\zeta=1$ for one parabolic segment of the chaotic saddle with $\tilde{\mu}_0=1$ and one stripe of the pseudobasin; $q_1=6\times10^{-4}$, $q_c=0$ and the stripe width $b=0.01\gg2q_1$ (dotted line), $b=2.8\times10^{-3}>2q_1$ (dashed line), and $b=3.6\times10^{-4}\ll2q_1$ (solid line). (b) Corresponding curves $MT_0|P_1|^2$ vs q_0+q_1. (c) Corresponding curves $\langle\tau\rangle$ vs q.

is a typical maximum observed also in systems with nonfractal basins of attraction; e.g., in many one-dimensional maps [4,10,11]. For smaller b the effects of touching the upper border of the stripe by the top of the parabola become visible. First, $\langle\tau\rangle$ decreases with q only within the interval between $q=0$ and $q=b$ and then increases with q (point B). Second, $|P_1|^2$ drops rapidly at $q_0+q_1=b$ (point B) and a second small maximum corresponding to the increasing branch of $\langle\tau(q)\rangle$ appears (point C). The SNR follows the behavior of $|P_1|^2$, with a sudden drop at $q_0+q_1=b$ (point B) and a secondary maximum (point C). If $b>2q_1$ a smooth maximum of both $|P_1|^2$ and the SNR at q_0 slightly above zero is still present (point A). However, if $b\ll2q_1$ the local minimum of $|P_1|^2$ and the SNR together with the second maximum (point E) shift to the left and cut off the first maximum turning it into a sharp one at $q_0+q_1=b$ (point D). The cutoff of the SNR corresponds again to the beginning of the increase of $\langle\tau\rangle$ at $q=b$ and decrease of $|P_1|^2$ (point D).

If more stripes of the pseudobasin were taken into account, the oscillating top of the parabola after leaving the first stripe would enter the next one with increasing q_0 and the SNR would increase again. The above example shows the connection between the shape of the curve SNR vs B_0 with multiple maxima, observed in Sec. III, and the oscillations of the mean time between jumps between the two parts of the postcritical attractor $\langle\tau\rangle$ (for a more detailed discussion see Appendix A). However, it should be also observed that the value of the numerator rather than the denominator in Eq. (9) determines the exact shape of the SNR curve. In general the SNR results from the superposition of many basic events like in examples above occurring simultaneously on different scales. This yields a complex structure like, e.g., in Fig. 3(a).

V. COMPARISON BETWEEN NUMERICAL AND THEORETICAL RESULTS

In this section we compare the predictions of the theory from Sec. IV with the numerical results. To do this we employ the model (10),(11) with parameters (given in Fig. 7) obtained similarly as in [32,33] for the estimation of $\langle\tau\rangle$. We identify the parameters q_0 and q_1 from the model of Sec. IV with B_0-B_c and B_1 in Eq. (7), respectively. For the abovementioned parameters the theoretical values of $\langle\tau\rangle$ vs B agree well with the numerically obtained ones [Fig. 7(a)]. The agreement is good for very small $B-B_c$, while in the region $B-B_c\geqslant10^{-4}$ a discrepancy between the numerical and theoretical results appears. Consequently, our theoretical results for the SNR obtained from Eq. (9), which are in quantitative agreement with the numerical ones in the limit $B_0+B_1\rightarrow B_c$, for larger B_0 reproduce the actual SNR only qualitatively.

In Figs. 7(b)–7(d) the numerical (solid) and theoretical (dashed) curves SNR vs B_0 are shown for slow periodic signal with $T_0=1024$ and three different amplitudes $B_1=3\times10^{-4}$, $B_1=6\times10^{-4}$ [cf. Fig. 3(a)], and $B_1=1.5\times10^{-3}$ (cf. Fig. 4). In all cases qualitative agreement between the theoretical and numerical results can be found. The best fit is observed for $B_1=3\times10^{-4}$ and small $B_0+B_1-B_c$ [Fig. 7(b)], where both the position and height of the segments close to the first strong maximum is predicted correctly by our theory. For larger B_1, in Fig. 7(c) and Fig. 7(d) the position of the segments and the order of magnitude of the height of local maxima close to the first strong maximum are predicted only approximately. As B_0 is increased, deviations between the numerical and theoretical curves for all B_1 in Figs. 7(b)–7(d) become significant.

It should be noted that small separate maxima that exist for small B_1 [Fig. 7(b)] for increasing B_1 merge or turn into plateaus close to strong maxima [Figs. 7(c) and 7(d)]. This effect is also qualitatively predicted by our theory. It occurs, since for large B_1 the oscillating top of the chaotic saddle sweeps several stripes of the pseudobasin of the other saddle.

In Fig. 8 the numerical and theoretical curves SNR vs B_0 are shown for $B_1=1.5\times10^{-3}$ and for a range of B_0 much wider than in Fig. 7(d). The numerically obtained maxima for large B_0 are small, although they still appear in certain groups. This is a reflection of the fuzzy fractal structure of chaotic saddles and their pseudobasins. In contrast, the the-

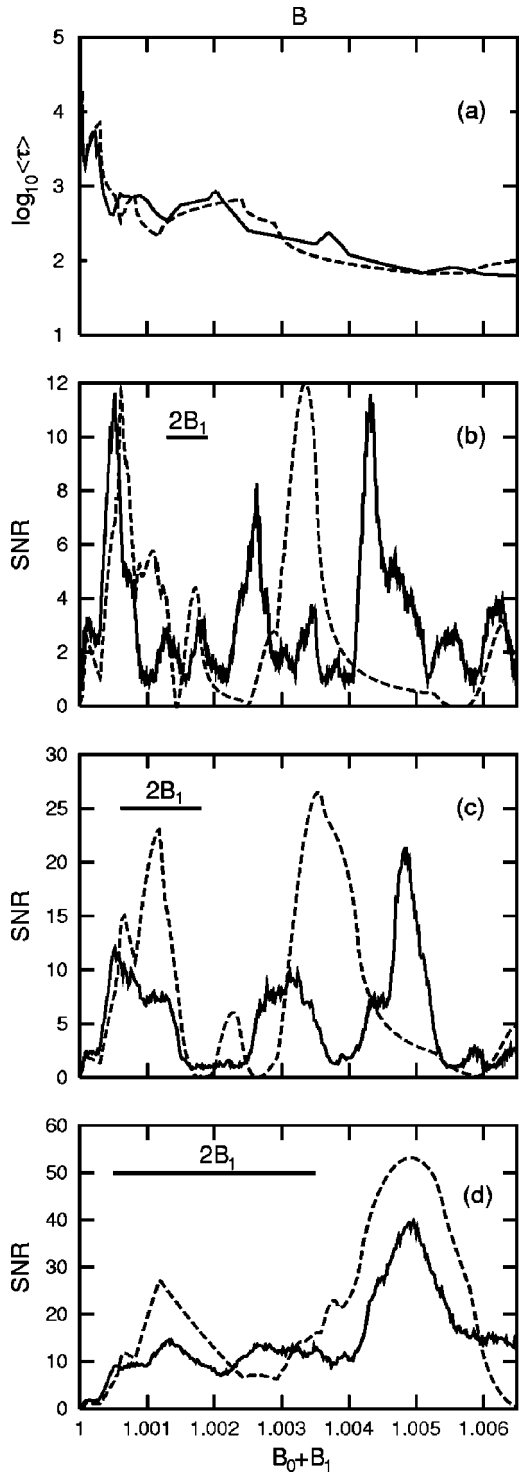

FIG. 7. (a) The mean time between jumps between symmetric parts of the attractor $\langle \tau \rangle$ vs B for the spin map (6) with parameters as in Fig. 1. Numerical results are shown with solid line and theoretical results obtained from the theory of Sec. IV B with $\alpha = 0.0108$, $\gamma = 0.294$, $\beta = 0.125$, $b_E = 1.467\,93$, $a/b = 1.667$, $\zeta = 3.33$, and $K = L = 10$—with dashed line. (b)–(d) The SNR vs $B_0 + B_1$ for the signal y_n from the spin map (6) with parameters as in Fig. 1 and $T_0 = 1024$: (b) $B_1 = 3 \times 10^{-4}$, (c) $B_1 = 6 \times 10^{-4}$, (d) $B_1 = 1.5 \times 10^{-3}$. The solid lines show numerical results. The dashed lines show theoretical results evaluated from Eq. (9) with the parameters of the theory of Sec. IV B as in (a).

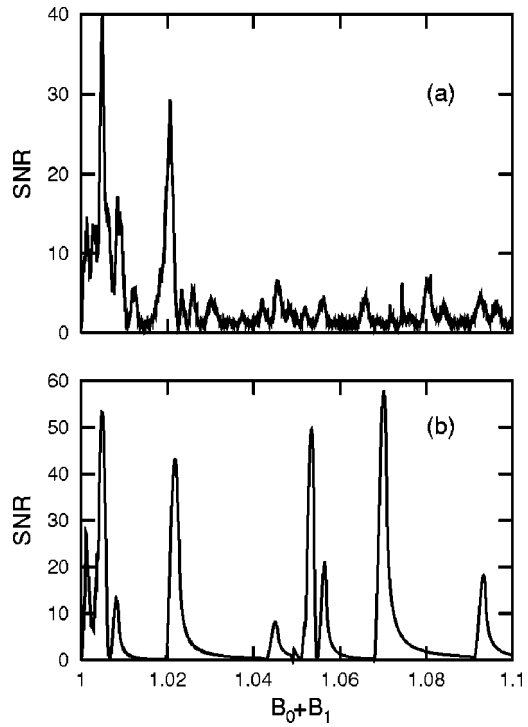

FIG. 8. The SNR vs $B_0 + B_1$ for the signal y_n from the spin map (6) with parameters as in Fig. 1 and $B_1 = 1.5 \times 10^{-3}$, $T_0 = 1024$ [extension of Fig. 7(d)]; (a) numerical results, (b) theoretical results evaluated from Eq. (9) with the parameters of the theory of Sec. IV B as in Fig. 7(a).

oretical curve shows a series of strong maxima, since in the model of Sec. IV the fractal structure of saddles and pseudobasins remains unchanged even for large B_0. Thus our theoretical model becomes inadequate for the description of SR in our system for B_0 much above B_c.

At this point the correspondence between the origin of stochastic multiresonance in systems with external noise [17,18] and noise-free stochastic multiresonance in the system (6) should be emphasized. In the former case multiresonance occurs, since in certain potentials the escape rate from the potential wells is the same for a discrete set of noise intensities [17,18]. Similarly, in our case, the rate of jumps between two parts of the postcritical attractor $\langle \tau \rangle^{-1}$ shows an oscillatory structure [Figs. 3(b) and 7(a)] as a function of B. Thus in both cases the main source of stochastic multiresonance is the nonmonotonic, oscillatory behavior of the rate of events forming the output signal from which the SNR is obtained as a function of the noise intensity or the control parameter.

VI. SUMMARY AND CONCLUSIONS

In this paper we reported the phenomenon of noise-free stochastic multiresonance in a chaotic spin map with periodically modulated control parameter in the vicinity of an attractor merging crisis. As the control parameter is varied, multiple strong maxima and other segments like plateaus and small local maxima in the output SNR appear. It was shown both numerically and theoretically that the multiresonance

appears due to the fractal structures of the precritical attractors and the fractal basins of attraction of the symmetric precritical attractors that collide at the crisis threshold. The adiabatic theory combined with a model for crisis in such a situation [32,33] yields the SNR curves that are in qualitative agreement with numerical results. The best fit is obtained for small amplitudes of the periodic signal and just above the threshold for crisis. Comparing with the case of stochastic multiresonance with external noise [17,18] our SNR curves show more complicated structure, the location of maxima is irregular and their magnitude decreases for large values of the control parameter. This irregularity is connected with incommensurability of the fractal structures of chaotic saddles and their pseudobasins, and with the disappearance of these structures as the control parameter is increased. However, in both cases the origin of the multiresonance is similar, namely, the invariance of the escape (jumping) rate for a discrete set of values of the noise intensity or the control parameter.

A sufficient condition for the occurrence of noise-free stochastic multiresonance should be the presence of oscillations of the average transient time $\langle \tau \rangle$ as the control parameter is varied. In this paper we used the kicked spin map as a model system that exhibits noise-free stochastic multiresonance, since in this case the anomalous oscillations of $\langle \tau \rangle$ are well pronounced and thus the multipeaked structure of the SNR is well visible. On the other hand, oscillations of the average transient time, although weaker, were observed in many systems with crises [43,44]. Thus the results of the present paper suggest that noise-free stochastic multiresonance can be observed also in other chaotic systems close to crisis, including experimental ones with continuous time.

ACKNOWLEDGMENTS

The authors are grateful to Professor V. S. Anishchenko for valuable discussions and U. Erdmann for discussions and help in numerical simulations. S. M., J. H., and W. E. were partly supported by special funds of the DFG, SFB 555 Komplexe Nichtlineare Prozesse. S. M. was also supported by the SOCRATES program of the European Community.

APPENDIX A: HEURISTIC RULES RELATING THE FUNCTIONS SNR VS B_0 AND $\langle \tau \rangle$ VS B

Let us define a ''segment'' in Figs. 3(a) and 3(b) as a region of monotonic behavior of the corresponding curve SNR vs B_0 or $\langle \tau \rangle$ vs B. For B_0+B_1 close to B_c the following relationships between the corresponding segments in Figs. 3(a) and 3(b) hold. First, the beginnings and ends of the narrow segments in Figs. 3(a) and 3(b), whose width is small compared to $2B_1$, correspond to each other. Second, if the width of the falling segment in Fig. 3(b) is larger than $2B_1$ then a maximum of the SNR in Fig. 3(a) occurs at B_0 slightly above the beginning of the segment in Fig. 3(b). Henceforth the values of B that separate the neighboring segments in Fig. 3(b), labeled as s, r, will be denoted as $B^{s,r}$. From Fig. 3(b) we obtain $B^{1,a} \approx 1.000\,22$, $B^{a,2} \approx 1.0005$, $B^{2,b} \approx 1.001$, $B^{b,3} \approx 1.001\,35$, $B^{3,c} \approx 1.002$. Then, according to the first rule, e.g., the plateau 1 in Fig. 3(a) occurs for $1.000\,09 < B_0+B_1 < B^{1,a} \approx 1.000\,22$ and the falling segment 2 for $1.0005 \approx B^{a,2} < B_0+B_1 < B^{2,b} \approx 1.001$. Similarly, the rising segment a occurs for $1.000\,22 \approx B^{1,a} < B_0+B_1 < B^{a,2} \approx 1.0005$ and the local maximum b for $1.001 \approx B^{2,b} < B_0+B_1 < B^{b,3} \approx 1.001\,35$. According to the second rule, e.g., the maximum c in Fig. 3(a) occurs at $B_0 \approx 1.0026 \approx B^{3,c}+B_1$.

It should be noted that the above-mentioned relationships can be understood on the basis of the simple example discussed in Sec. IV C. Let us try to justify the first rule. E.g., a narrow oscillation of $\langle \tau \rangle$ in Fig. 3(b) is the one with segments 1, a, and 2, and the width of its falling segment a is $B^{a,2}-B^{1,a} = 2.8 \times 10^{-4} \ll 2B_1 = 1.2 \times 10^{-3}$. The beginning of the falling segment $B^{1,a}$ in the example from Sec. IV C corresponds to $q=0$ and its end $B^{a,2}$ to $q=b$. It follows from Sec. IV C that a sharp maximum of the SNR should appear at $B_0+B_1 \approx B^{a,2} \approx 1.0005$, which is in accordance with Fig. 3(a). To the left of the maximum the increase of the SNR should be observed, i.e., for $B^{1,a} \approx 1.000\,22 < B_0+B_1 < B^{a,2}$ [segment a in Fig. 3(a)]. To the right of the maximum the decrease of the SNR should be observed, i.e., for $B_0+B_1 > B^{a,2}$ [segment 2 in Fig. 3(a)]. This is again in agreement with the numerical results in Sec. III and with the first heuristic rule above. Now, let us consider the second rule. A wide falling segment in Fig. 3(b) is the segment c, whose width is greater than $2B_1$. The beginning of this segment $B^{3,c}$ in the example from Sec. IV C corresponds to $q=0$, thus a smooth maximum of the SNR should appear at B_0 slightly above $B_0 = B^{3,c} \approx 1.002$, again close to its true position at $B_0 \approx 1.0026$ in Fig. 3(a) and close to the prediction of the second heuristic rule above. The secondary maxima of the SNR that in Fig. 6(a) correspond to the top of the parabolic segment leaving the stripe of the pseudobasin cannot be seen in Fig. 3(a), since the amplitude of periodic modulation is so large that they merged with the broad maxima.

APPENDIX B: EVALUATION OF THE FUNCTIONS IN THE ANALYTIC FORMULA FOR THE SNR

The measure of the overlap of the parabolic segment $\mathcal{A}_k$ and the half-plane $y>c$ can be for small $q_0+q_1\cos\omega_0 n - (1-\delta_{k,K+1}) a\alpha^k - c$ approximated as

$$\mu_k[c,n] = \tilde{\mu}_k \sqrt{q_0+q_1\cos\omega_0 n-(1-\delta_{k,K+1})a\alpha^k-c} \times \Theta[q_0+q_1\cos\omega_0 n - a(1-\delta_{k,K+1})\alpha^k - c], \tag{B1}$$

where $\Theta(\,)$ is the Heaviside step function. It follows that $\mu_k[c,n]$ is an even, periodic function of n. Its time average $\overline{\mu_k}(c)$ and its first Fourier coefficient $M_{k,1}(c)$ can be evaluated analytically in the continuous time approximation $n \to t$.

To do this let us again consider the function (B1). The overlap of the kth parabolic segment and the half-plane $y>c$ is nonzero during at least a part of the period T_0 if the control parameter fulfils the condition $q_0 > q_{0,min} = c + (1-\delta_{k,K+1}) a\alpha^k - q_1$. The overlap is nonzero during the whole period if $q_0 > q_{0,full} = c + (1-\delta_{k,K+1}) a\alpha^k + q_1$. Let us introduce the time $t_k(c)$ defined so that $\mathcal{A}_k$ overlaps the half-plane $y>c$ for $0 \leqslant t < t_k(c)$ and $T_0 - t_k(c) < t \leqslant T_0$, i.e.,

$$t_k(c)=\begin{cases}\omega_0^{-1}\arccos\{[c-q_0+(1-\delta_{k,K+1})a\alpha^k]/q_1\} & \text{if } q_{0,min}\leqslant q_0\leqslant q_{0,full}\\ T_0/2 & \text{if } q_0>q_{0,full}.\end{cases} \quad \text{(B2)}$$

Let us also introduce the quantity

$$m_k(c)=\sqrt{2q_1/[q_0-(1-\delta_{k,K+1})a\alpha^k+q_1-c]}. \quad \text{(B3)}$$

The time average of the function $\mu_k[c,t]$ [Eq. (B1)] can be then evaluated as

$$\begin{aligned}\overline{\mu}_k(c)&=\frac{1}{T_0}\int_0^{T_0}\mu_k[c,t]dt\\ &=\frac{2\tilde{\mu}_k}{\pi}\sqrt{q_0+q_1-(1-\delta_{k,K+1})a\alpha^k-c}\\ &\times E\left[\frac{\omega_0}{2}t_k(c),m_k(c)\right]\\ &\times\Theta[q_0+q_1-(1-\delta_{k,K+1})a\alpha^k-c]. \quad \text{(B4)}\end{aligned}$$

Here $E(\phi,m)=\int_0^{\phi}(1-m^2\sin^2x)^{1/2}dx$ is the elliptic integral of the second kind.

Similarly, the first Fourier coefficient $M_{k,1}(c)$ of the function $\mu_k[c,t]$ [Eq. (B1)] can be evaluated as

$$\begin{aligned}M_{k,1}(c)&=\frac{1}{T_0}\int_0^{T_0}\mu_k[c,t]\cos\omega_0 t dt\\ &=\frac{2\tilde{\mu}_k}{\pi}\sqrt{q_0+q_1-(1-\delta_{k,K+1})a\alpha^k-c}\\ &\times\left\{\frac{2-m_k^2(c)}{3m_k^2(c)}E\left[\frac{\omega_0}{2}t_k(c),m_k(c)\right]\right.\\ &\left.-\frac{2-2m_k^2(c)}{3m_k^2(c)}F\left[\frac{\omega_0}{2}t_k(c),m_k(c)\right]\right\}\\ &\times\Theta[q_0+q_1-(1-\delta_{k,K+1})a\alpha^k-c]. \quad \text{(B5)}\end{aligned}$$

Here $F(\phi,m)=\int_0^{\phi}(1-m^2\sin^2x)^{-1/2}dx$ is the elliptic integral of the first kind.

We emphasise that in Eqs. (B4) and (B5) the control parameter q_0 appears not only via the square root but also via the functions t_k [Eq. (B2)] and m_k [Eq. (B3)], which also depend on q_0 in a complicated way. It should be also noted that if $q_0>q_{0,full}$ then $\omega_0 t_k(c)/2=\pi/2$ and the elliptic integrals in Eqs. (B4),(B5) change into complete elliptic integrals. Besides, the results for $\overline{\mu}_k(c)$, $M_{k,1}(c)$ do not depend on ω_0 since in Eqs. (B4) and (B5) ω_0 cancels with ω_0^{-1} in the definition of $t_k(c)$ [Eq. (B2)].

The expressions for the coefficients $\overline{\mu}_{kl}$ and $M_{kl,1}$ in Eq. (15) in Sec. IV B can be obtained from Eqs. (B4) and (B5), respectively. For this purpose one should use the definition of $\mu_{kl}(n)$ [Eq. (14)] and replace c in Eq. (B4) and Eq. (B5) by $(1-\delta_{l,L+1})(\beta^l b-\beta^l b_E)$ or $\beta^l b$.

[1] R. Benzi, A. Sutera, and A. Vulpiani, J. Phys. A **14**, L453 (1981).
[2] L. Gammaitoni, P. Hänggi, P. Jung, and F. Marchesoni, Rev. Mod. Phys. **70**, 223 (1998).
[3] V.S. Anishchenko, A.B. Neiman, F. Moss, and L. Schimansky-Geier, Phys. Usp. **42**, 7 (1999) [Usp. Fiz. Nauk **169**, 7 (1999)].
[4] V.S. Anishchenko, A.B. Neiman, and M.A. Safanova, J. Stat. Phys. **70**, 183 (1993).
[5] G. Nicolis, C. Nicolis, and D. McKernan, J. Stat. Phys. **70**, 125 (1993).
[6] T.L. Carroll and L.M. Peccora, Phys. Rev. Lett. **70**, 576 (1993).
[7] T.L. Carroll and L.M. Peccora, Phys. Rev. E **47**, 3941 (1993).
[8] A. Crisanti, M. Falcioni, G. Paladin, and A. Vulpiani, J. Phys. A **27**, L597 (1994).
[9] A. Krawiecki, Acta Phys. Pol. A **92**, 1101 (1997).
[10] A. Krawiecki and A. Sukiennicki, Chaos **8**, 768 (1998).
[11] S. Sinha and B.K. Chakrabarti, Phys. Rev. E **58**, 8009 (1998).
[12] S. Sinha, Physica A **270**, 204 (1999).
[13] Changsong Zhou and C.-H. Lai, Phys. Rev. E **60**, 3928 (1999).
[14] V.S. Anishchenko, M.A. Safonova, and L.O. Chua, Int. J. Bifurcation Chaos Appl. Sci. Eng. **4**, 441 (1994).
[15] E. Reibold, W. Just, J. Becker, and H. Benner, Phys. Rev. Lett. **78**, 3101 (1997).
[16] P. Jung and P. Hänggi, Phys. Rev. A **44**, 8032 (1991).
[17] J.M.G. Vilar and J.M. Rubí, Phys. Rev. Lett. **78**, 2882 (1997).
[18] J.M.G. Vilar and J.M. Rubí, Physica A **264**, 1 (1999).
[19] B. NcNamara, K. Wiesenfeld, and R. Roy, Phys. Rev. Lett. **60**, 2626 (1988).
[20] B. McNamara and K. Wiesenfeld, Phys. Rev. A **39**, 4854 (1989).
[21] P. Jung and P. Hänggi, Europhys. Lett. **8**, 505 (1989).
[22] K. Wiesenfeld, D. Pierson, E. Pantazelou, Ch. Dames, and F. Moss, Phys. Rev. Lett. **72**, 2125 (1994).
[23] Z. Gingl, L.B. Kiss, and F. Moss, Europhys. Lett. **29**, 191 (1995).
[24] K. Loerincz, Z. Gingl, and L.B. Kiss, Phys. Lett. A **224**, 63

(1996).
[25] F. Chapeau-Blondeau, Phys. Rev. E **53**, 5469 (1995).
[26] F. Chapeau-Blondeau and X. Godivier, Phys. Rev. E **55**, 1478 (1997).
[27] M.M. Alibegov, Phys. Rev. E **59**, 4841 (1999).
[28] H.E. Plesser and T. Geisel, Phys. Rev. E **59**, 7008 (1999).
[29] J.A. Hołyst and A. Sukiennicki, Acta Phys. Pol. A **81**, 353 (1992).
[30] J.A. Hołyst and A. Sukiennicki, J. Magn. Magn. Mater. **104-107**, 2111 (1992).
[31] K. Kacperski and J.A. Hołyst, Phys. Rev. E **55**, 5044 (1997).
[32] K. Kacperski and J.A. Hołyst, Phys. Lett. A **254**, 53 (1999).
[33] K. Kacperski and J.A. Hołyst, Phys. Rev. E **60**, 403 (1999).
[34] S. Matyjaśkiewicz, J.A. Hołyst, and A. Krawiecki, Phys. Rev. E **61**, 5134 (2000).
[35] C. Grebogi, E. Ott, F. Romeiras, and J.A. Yorke, Phys. Rev. A **36**, 5365 (1987).
[36] J.R. Friedman, M.P. Sarachik, J. Tejada, and R. Ziolo, Phys. Rev. Lett. **76**, 3830 (1996).
[37] E. M. Chudnovsky and J. Tejada, *Macroscopic Quantum Tunneling of the Magnetic Moment* (Cambridge University Press, Cambridge, England, 1998).
[38] M. Kuś, R. Scharf, and F. Haake, Z. Phys. B **66**, 129 (1987).
[39] M. Kuś, F. Haake, and B. Eckhardt, Z. Phys. B **92**, 221 (1993).
[40] P. Gerwinski, F. Haake, H. Wiedemann, M. Kuś, and K. Życzkowski, Phys. Rev. Lett. **74**, 1562 (1995).
[41] A.N. Grigorenko, P.I. Nikitin, A.N. Slavin, and P.Y. Zhou, J. Appl. Phys. **76**, 6335 (1994).
[42] A.N. Grigorenko, V.I. Konov, and P.I. Nikitin, JETP Lett. **52**, 593 (1990) [Pis'ma Zh. Eksp. Teor. Fiz. **52**, 1182 (1990)].
[43] C. Grebogi, E. Ott, and J.A. Yorke, Phys. Rev. Lett. **57**, 1284 (1986).
[44] J.C. Sommerer and C. Grebogi, Int. J. Bifurcation Chaos Appl. Sci. Eng. **2**, 383 (1992).